Toroidal grating astigmatism of high-harmonics characterized by EUV Hartmann sensor

Tobias Mey,[1*] **Sergey Zayko,**[2] **Claus Ropers,**[2] **Bernd Schäfer,**[1] **and Klaus Mann**[1]

[1] *Laser-Laboratorium Göttingen e.V., Hans-Adolf-Krebs-Weg 1, 37077 Göttingen, Germany*
[2] *Universität Göttingen, Friedrich-Hund-Platz 1, 37077 Göttingen, Germany*

[*] *tobias.mey@llg-ev.de*

Abstract: The beam transport of single high-order harmonics in a monochromator arrangement is studied. A toroidal grating combines spectral filtering and focusing in order to produce a small individual spot for each harmonic. Here, the effect of small deviations from perfect alignment is investigated. Experimentally, a Hartmann sensor monitors the EUV wavefront while the grating is subjected to an online alignment procedure. The obtained results are confirmed by a simple theoretical description employing optical matrix methods.

OCIS codes: (050.1950) Diffraction gratings; (080.2730) Matrix methods in paraxial optics; (140.3295) Laser beam characterization; (340.7480) X-rays, soft x-rays, extreme ultraviolet (EUV).

References and links

1. A. McPherson, G. Gibson, H. Jara, U. Johann, T. S. Luk, I. A. McIntyre, K. Boyer, and C. K. Rhodes, "Studies of multiphoton production of vacuum-ultraviolet radiation in the rare gases," JOSA B **4,** 595–601 (1987).
2. T. Pfeifer, C. Spielmann, and G. Gerber, "Femtosecond x-ray science," Rep. Prog. Phys. **69,** 443 (2006).
3. D. G. Stearns, R. S. Rosen, and S. P. Vernon, "Multilayer mirror technology for soft-x-ray projection lithography," Appl. Opt. **32,** 6952–6960 (1993).
4. M. Schultze, E. Goulielmakis, M. Uiberacker, M. Hofstetter, J. Kim, D. Kim, F. Krausz, and U. Kleineberg, "Powerful 170-attosecond XUV pulses generated with few-cycle laser pulses and broadband multilayer optics," New J. Phys. **9,** 243 (2007).
5. M. Hutley, *Diffraction Gratings* (Academic Press Inc., 2009).
6. B. Schäfer, and K. Mann, "Investigation of the propagation characteristics of excimer lasers using a HartmannShack sensor," Rev. Sci. Instr. **71,** 2663–2668 (2000).
7. B. Schäfer, M. Lübbecke and K. Mann, "Hartmann-Shack wave front measurements for real time determination of laser beam propagation parameters," Rev. Sci. Instr. **77,** 053103 (2006).
8. B. Flöter, P. Juranić, S. Kapitzki, B. Keitel, K. Mann, E. Plönjes, B. Schäfer, and K. Tiedtke, "EUV Hartmann sensor for wavefront measurements at the Free-electron LASer in Hamburg," New J. Phys. **12,** 083015 (2010).
9. B. Flöter, P. Juranić, P. Großmann, S. Kapitzki, B. Keitel, K. Mann, E. Plönjes, B. Schäfer, and K. Tiedtke, "Beam parameters of FLASH beamline BL1 from Hartmann wavefront measurements," Nucl. Instrum. Meth. A **635,** S108–S112 (2011).
10. B. L. Henke, E. M. Gullikson, and J. C. Davis, "X-Ray Interactions: Photoabsorption, Scattering, Transmission, and Reflection at E = 50-30,000 eV, Z = 1-92," At. Data Nucl. Data Tables **54,** 181–342 (1993).
11. B. Flöter, "Strahlcharakterisierung von Freie-Elektronen-Lasern im weichen Röntgen-Spektralbereich," PhD thesis, Universität Göttingen (2012).
12. D. Attwood, *Soft X-Rays and Extreme Ultraviolet Radiation* (Cambridge University Press, 1999).
13. E. Hecht, *Optics* (Pearson Education Limited 2014).
14. H. A. Padmore, "Optimization of soft x-ray monochromators (invited)," Rev. Sci. Instrum. **60,** 1608–1615 (1989).
15. Q. Xue, S. Wang, and F. Lu, "Aberration-corrected Czerny-Turner imaging spectrometer with a wide spectral region," Appl. Opt. **48,** 11–16 (2009).

#235328 - $15.00 USD Received 27 Feb 2015; revised 21 May 2015; accepted 25 May 2015; published 2 Jun 2015

16. T. Harada and T. Kita, "Mechanically ruled aberration-corrected concave gratings," Appl. Opt. **19,** 3987–3993 (1980).
17. *ISO 11146-1: Lasers and laser-related equipment - Test methods for laser beam widths, divergence angle and beam propagation ratio Part 1: Stigmatic and simple astigmatic beams* (2003).
18. D. T. Lloyd, K. O'Keeffe, and S. Hooker, "Complete spatial characterization of an optical wavefront using a variable-separation pinhole pair," Opt. Lett. **38,** 1173–1175 (2013).
19. B. Eppich, "Die Charakterisierung von Strahlungsfeldern mit der Wigner-Verteilung und deren Messung," PhD thesis, Technische Universität Berlin (1998).
20. A. E. Siegman, "ABCD-matrix elements for a curved diffraction grating," JOSA A **2,** 1793 (1985).

1. Introduction

The high-harmonic generation (HHG) process converts electromagnetic radiation into integer multiples of the fundamental frequency reaching EUV and soft x-ray wavelengths [1,2]. All individually quasi-monochromatic harmonics propagate collinearly with the incident laser beam. In order to prepare a beam which contains only a few or even single harmonics, multilayer mirrors with a wavelength-selective reflectivity are commonly used [3, 4]. Similarly, a reflection grating acts on the HHG beam by separating the harmonics into different diffraction angles [5]. Both techniques can be combined with curved surfaces to refocus the divergent HHG radiation to a probe position. However, such devices are highly sensitive to slight misalignments of, e.g., the angle of incidence. As a result, aberrations lead to an increased focal spot diameter and a reduced intensity. Moreover, the phase distribution becomes distorted, which limits the applicability of the EUV radiation in phase retrieval applications such as coherent diffractive imaging. This creates the need for a highly precise alignment of the involved optical elements.

Hartmann type sensors are known to be versatile tools for optics alignment in the visible and UV spectral range [6, 7]. The wavefront distribution is derived from single exposures in terms of a composition of specific aberrations. This allows for an online wavefront monitoring and thus for an adjustment of the related optics in the beam path. Recently, similar applications have been successfully demonstrated in the EUV range, too, where an ellipsoidal focusing optic is aligned with an unprecedented precision [8, 9].

In this work, the propagation of single harmonics is studied after passing a toroidal grating that combines spectral filtering and focusing. A Hartmann sensor captures the EUV wavefront while the angle of incidence of the harmonic on the grating is varied. Here, already tiny variations lead to a significant impact, especially influencing the astigmatic aberration. Beyond the experimental characterization, the observed effect is described theoretically by matrix methods. Both methods agree well to each other and an optimum angle of incidence is found, at which aberrations are minimized.

2. Experimental

The setup of the investigated HHG source is schematically depicted in figure 1. A titanium sapphire laser generates ultra-short pulses of near-infrared radiation which are focused into an argon filled capillary (pulse energy 0.5 mJ, pulse length 40 fs, center wavelength 800 nm, repetition rate 1 kHz). In the noble gas, the highly non-linear HHG process results in odd harmonics, measured up to the 51^{st} order. After the conversion, the fundamental beam is absorbed by a mesh-less aluminum filter of 200 nm thickness, whereas radiation in the wavelength range $17\,\text{nm} \lesssim \lambda \lesssim 80\,\text{nm}$ is transmitted [10]. A toroidal grating generates a row of individual foci for each harmonic (sagittal radius $R_s = 104.9\,\text{mm}$, tangential radius $R_t = 1000\,\text{mm}$, constant groove density $g = 550\,\text{mm}^{-1}$, focal length in 0. order $f_{\text{tor}} = 160\,\text{mm}$, manufactured by Jobin Yvon Inc.). In the -1. diffraction order, a slit allows for propagation of single harmonics while all others are blocked. Within the scope of the present study, the 25^{th} harmonic is selected, corresponding to a wavelength of $\lambda = 32\,\text{nm}$.

#235328 - $15.00 USD Received 27 Feb 2015; revised 21 May 2015; accepted 25 May 2015; published 2 Jun 2015

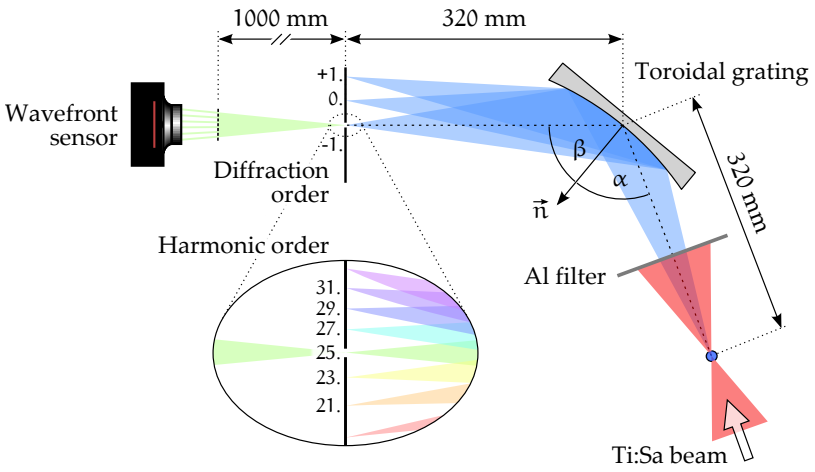

Fig. 1. Setup of HHG source with a single toroidal grating acting as monochromator. $\vec{n}$ denotes the normal vector of the toroidal surface.

The Hartmann sensor is a combination of a CCD chip (1392×1040 square pixels, size $6.5\,\mu$m, dynamic range 14 bit) with a pinhole array in a distance of 95 mm to the chip (pinhole diameter $75\,\mu$m, pinhole pitch $250\,\mu$m). The detector is placed 1000 mm behind the expected focal position of the HHG beam. In order to accumulate a sufficient signal, an exposure time of 40 s is selected.

The EUV beam is divided by the pinhole array into many small sub-beams, which then individually propagate in the direction of the local Poynting vector, each producing a spot on the CCD chip. The wavefront is then reconstructed by a comparison between the resulting spot distribution and a reference distribution corresponding to a plane wave illumination with Gaussian spots separated by $250\,\mu$m in the horizontal and vertical direction. Generally, this pattern is approximated by an elementary wave as resulting from a small pinhole [8]. Here, due to the low HHG intensity, the reference distribution had to be generated synthetically.

In case of coherent radiation, the information obtained by the Hartmann sensor allows for the calculation of beam propagation parameters, e.g., the horizontal and vertical waist positions [8]. In the following, the distance between both positions Δz, i.e. the waist difference, will be used as a measure for the astigmatic aberration. A detailed description of the principle of the employed sensor is found in [9, 11].

During online monitoring of the wavefront, the angle of incidence α between the HHG beam and the normal of the toroid is increased in steps of $\Delta\alpha = 0.05°$. The deflection angle β changes according to the grating equation [12]

$$\sin\beta - \sin\alpha = m\,g\,\lambda, \tag{1}$$

with the diffraction order m and groove density g. In the course of this alignment procedure, the effective radius of the optic decreases in the tangential direction, and it increases in the sagittal direction [13]. As a consequence, the beam experiences a stronger horizontal focusing and a weaker vertical focusing. For a certain angle α_0, both focal distances are equal to each other and the foci coincide. A selection of three wavefronts captured at different angles α is depicted in Figure 2.

Apparently, already small variations of the angle of incidence lead to a significant change of the astigmatic aberration. The curvature of the wavefront indicates that at an angle of incidence of $\alpha = 72.20°$, the beam is horizontally divergent and vertically convergent. At $\alpha = 72.95°$ the situation appears reversed. Thereby, the astigmatic waist difference Δz changes its value from

#235328 - $15.00 USD Received 27 Feb 2015; revised 21 May 2015; accepted 25 May 2015; published 2 Jun 2015

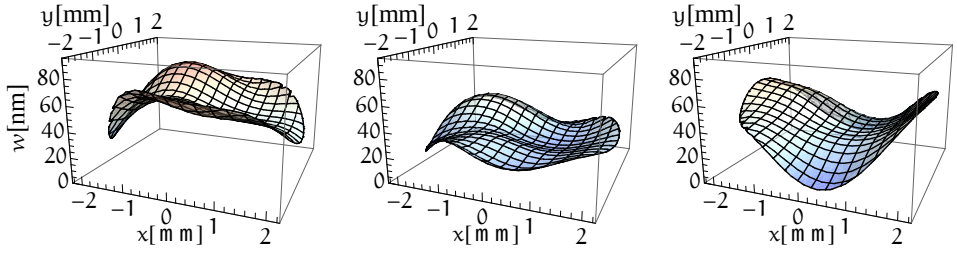

Fig. 2. HHG wavefront of the 25th harmonic, measured at different angles of incidence α. Tilt and defocus terms are subtracted, Δz denotes the astigmatic waist difference.

27 mm to −22 mm. In between, at $\alpha = 72.65^\circ$ the focusing of the optic is well balanced, and Δz vanishes.

Obviously, the optimized wavefront is not entirely flat due to remaining higher order aberrations. A corresponding Zernike analysis reveals that the strongest contribution is given by the coma aberration. In principle, this can be reduced by the use of apertures or schemes of aberration-corrected setups [14,15] which involve several optical components. With both strategies, the achievable flux reduces significantly. In contrast, there also exist aberration corrected toroidal gratings which, for a certain wavelength, compensate also the coma aberration [16].

3. Theoretical description

In the following, the astigmatic waist difference $\Delta z(\alpha)$ is theoretically estimated by matrix methods and then compared to the experimental results.

The fundamental laser beam is taken to be Gaussian with a local diameter of 8 mm before being focused by the lens into the argon filled capillary (focal length 200 mm). Thus, the divergence is $\approx 8/200 = 40$ mrad and with $M^2 = 1$, the focus diameter is derived to $d_0 = 25\,\mu$m [17]. The 25th harmonic is assumed to exhibit the same source diameter and a divergence which is 25 times smaller than that of the incident laser beam:

$$\begin{aligned} d_0 &= 25\,\mu\text{m} \\ \theta &= 1.6\,\text{mrad}. \end{aligned}$$

While a diffraction limited beam ($M^2 = 1$) is a reasonable assumption for the fundamental, this does not necessarily apply to the generated harmonics. In fact, the beam properties may vary for different harmonic orders, depending, e.g., on the phase matching conditions [18]. Thus, the beam quality factor might be larger which would mainly lead to an increased waist diameter after passing the toroid. However, for the following estimations of the waist difference this plays a minor role and can therefore be neglected.

With the given beam properties, the HHG beam matrix

$$\mathscr{M}_0 = \begin{pmatrix} \langle x^2 \rangle & \langle xy \rangle & \langle xu \rangle & \langle xv \rangle \\ \langle xy \rangle & \langle y^2 \rangle & \langle yu \rangle & \langle yv \rangle \\ \langle xu \rangle & \langle yu \rangle & \langle u^2 \rangle & \langle uv \rangle \\ \langle xv \rangle & \langle yv \rangle & \langle uv \rangle & \langle v^2 \rangle \end{pmatrix} \tag{2}$$

is derived at the source position, where all mixed moments vanish [19]. Now, ray transformation matrices as given in the appendix are applied to the beam matrix $\mathscr{M}_0$ corresponding

#235328 - $15.00 USD Received 27 Feb 2015; revised 21 May 2015; accepted 25 May 2015; published 2 Jun 2015

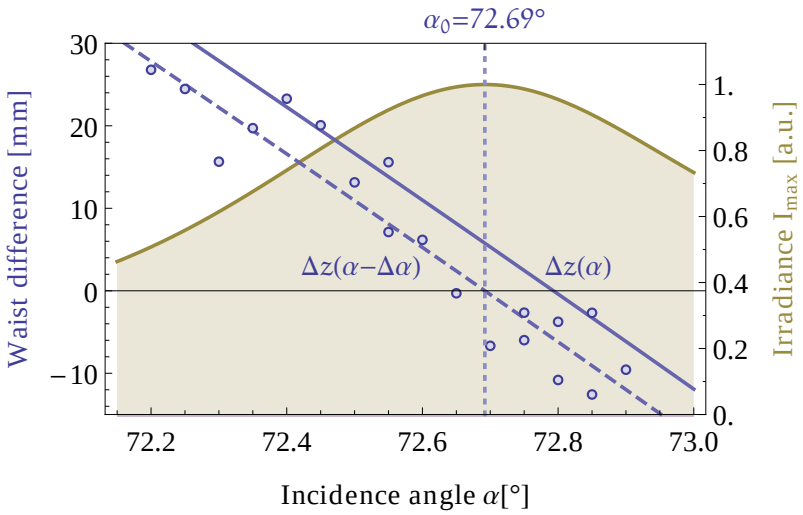

Fig. 3. Astigmatic waist difference plotted as a function of the angle of incidence. The theoretical curve $\Delta z(\alpha)$ (solid blue line) lies slightly above the experimental values (blue dots). With a shift of $\Delta\alpha = -0.1°$, best agreement is obtained (dashed blue line). The achievable irradiance $I_{\max}(\alpha)$ is derived with respect to that coordinate shift.

to the experimental situation. First, $\mathscr{M}_0$ is propagated to the optic by $\mathscr{S}_{\text{prop}}(320\,\text{mm})$. Then, the toroidal grating $\mathscr{S}_{\text{tg}}(\alpha)$ acts on the beam and a subsequent propagation by $\mathscr{S}_{\text{prop}}(z)$ finally yields the system matrix $\mathscr{S}(z,\alpha)$ that transforms a beam $\mathscr{M}_0$ from the source position to a distance z behind the optic:

$$\begin{aligned} \mathscr{S}(z,\alpha) &= \mathscr{S}_{\text{prop}}(z)\cdot\mathscr{S}_{\text{tg}}(\alpha)\cdot\mathscr{S}_{\text{prop}}(320\,\text{mm}) \\ \mathscr{M}(z,\alpha) &= \mathscr{S}(z,\alpha)\cdot\mathscr{M}_0\cdot\mathscr{S}(z,\alpha)^T. \end{aligned} \tag{3}$$

Here, the beam matrix is propagated to the detector position $z = 1320\,\text{mm}$. With $\mathscr{M}(1320\,\text{mm},\alpha)$ the waist positions $z_{0,x}(\alpha) = -\langle xu\rangle/\langle u^2\rangle$ and $z_{0,y}(\alpha) = -\langle yv\rangle/\langle v^2\rangle$ are derived, and the astigmatic waist difference $\Delta z(\alpha) = z_{0,x}(\alpha) - z_{0,y}(\alpha)$ is computed. The resulting function $\Delta z(\alpha)$ is depicted in figure 3 as a solid blue line together with the values resulting from the measured wavefronts.

The theoretical waist difference $\Delta z(\alpha)$ appears slightly above the experimental values. Although the relative angle of incidence is adjusted very precisely, its absolute value might contain a small error. A least squares fit routine results a deviation of $\Delta\alpha = -0.1°$. The resulting shifted function $\Delta z(\alpha - \Delta\alpha)$ is plotted in figure 3 in dashed style revealing good agreement with the measurement. The angle of incidence for a vanishing waist difference is derived to $\alpha_0 = 72.69°$. It is expected that for this angle the beam is focused into the smallest beam area. In the following, the achievable intensity depending on the angle of incidence is estimated in arbitrary units.

From matrix $\mathscr{M}(z,\alpha)$, the local beam diameters $d_x(z,\alpha)$ and $d_y(z,\alpha)$ are derived. Approximating the beam area $A(z,\alpha) = \frac{\pi}{4} d_x(z,\alpha)\, d_y(z,\alpha)$ by an ellipse, the mean irradiance at position z is $I(z,\alpha) = P_0/A(z,\alpha)$ with an arbitrary beam power P_0. For a specific angle of incidence α, the position $z_{\max}$ is derived which yields the maximum value of $I(z,\alpha)$. This achievable irradiance $I_{\max}(\alpha)$ is depicted together with the astigmatic waist difference in figure 3 including the coordinate shift $\Delta\alpha$.

As expected, the highest photon flux is obtained for an angle of incidence of $\alpha_0 = 72.69°$,

#235328 - $15.00 USD Received 27 Feb 2015; revised 21 May 2015; accepted 25 May 2015; published 2 Jun 2015

where the astigmatic aberration disappears. It is evident that already a small misalignment of 0.5° reduces the achievable intensity by 50% which renders this alignment relevant for imaging applications. Furthermore, phase distortions of the illumination function are minimized. With respect to coherent diffractive imaging experiments, this is mandatory: a successful reconstruction of phase objects can only be achieved if the phase distortions of the probe beam are negligible with respect to the sample.

4. Conclusion

With a Hartmann type wavefront sensor, the EUV beam transport is investigated at an HHG setup, where a toroidal grating achieves both spectral filtering and focusing. In an online adjustment, it is demonstrated that already small misalignments of the angle of incidence between EUV beam and toroidal grating lead to significant aberrations and a corresponding loss of intensity. A theoretical approach corroborates the results. For future phase retrieval experiments, this procedure is crucial in order to achieve a flat phase distribution at the sample position, effectively reducing reconstruction errors.

Appendix

The following ray propagation matrices are employed in this work [19, 20]:

$$\mathscr{S}_{\text{prop}}(z) = \begin{pmatrix} 1 & 0 & z & 0 \\ 0 & 1 & 0 & z \\ 0 & 0 & 1 & 0 \\ 0 & 0 & 0 & 1 \end{pmatrix} \quad ; \quad \mathscr{S}_{\text{tg}} = \begin{pmatrix} \frac{\cos\beta}{\cos\alpha} & 0 & 0 & 0 \\ 0 & 1 & 0 & 0 \\ -\frac{2}{R'_t} & 0 & \frac{\cos\alpha}{\cos\beta} & 0 \\ 0 & -\frac{2}{R'_s} & 0 & 1 \end{pmatrix} \tag{4}$$

where, z is a propagation distance, α and β are incidence and deflection angle relative to the gratings normal vector, and R'_t and R'_s are the effective tangential and sagittal radius, which are defined as

$$R'_t = \frac{2\cos\alpha\cos\beta}{\cos\alpha+\cos\beta}R_t \quad ; \quad R'_s = \frac{2}{\cos\alpha+\cos\beta}R_s \tag{5}$$

with the tangential and sagittal radius R_t and R_s.

Acknowledgments

We gratefully acknowledge support by Deutsche Forschungsgemeinschaft within SFB755 'Nanoscale Photonic Imaging' (project C08).

#235328 - $15.00 USD Received 27 Feb 2015; revised 21 May 2015; accepted 25 May 2015; published 2 Jun 2015